HHS Public Access

Author manuscript

Cell. Author manuscript; available in PMC 2019 March 22.

Published in final edited form as:

Cell. 2018 March 22; 173(1): 74–89.e20. doi:10.1016/j.cell.2018.02.008.

Impairment of an endothelial NAD$^+$-H_2S signaling network is a reversible cause of vascular aging

Abhirup Das[1,2,3,8], **George X. Huang**[1,4,8], **Michael S. Bonkowski**[1], **Alban Longchamp**[5], **Catherine Li**[2], **Michael B. Schultz**[1], **Lynn-Jee Kim**[2], **Brenna Osborne**[6], **Sanket Joshi**[6], **Yuancheng Lu**[1], **Jose Humberto Treviño-Villarreal**[5], **Myung-Jin Kang**[2], **Tzong-tyng Hung**[7], **Brendan Lee**[7], **Eric O. Williams**[3], **Masaki Igarashi**[3], **James R. Mitchell**[5], **Lindsay E. Wu**[2], **Nigel Turner**[6], **Zolt Arany**[4,*], **Leonard Guarente**[3,*], and **David A. Sinclair**[1,2,9,*]

[1]Paul F. Glenn Center for the Biological Mechanisms of Aging, Department of Genetics, Harvard Medical School, Boston, MA 02115, USA

[2]Laboratory for Ageing Research, Department of Pharmacology, School of Medical Sciences, The University of New South Wales, Sydney NSW 2052, Australia

[3]Paul F. Glenn Center for Science of Aging Research, Department of Biology, Massachusetts Institute of Technology, Cambridge, MA 02139, USA

[4]Cardiovascular Institute, Perelman School of Medicine, University of Pennsylvania, 3400 Civic Center Boulevard, Bldg. 421, Philadelphia, PA 19104, USA

[5]Department of Genetics and Complex Diseases, Harvard T. H. Chan School of Public Health, Boston, MA, USA

[6]Mitochondrial Bioenergetics Laboratory, Department of Pharmacology, School of Medical Sciences, The University of New South Wales, Sydney NSW 2052, Australia

[7]Biological Resources Imaging Laboratory, Mark Wainwright Analytical Centre, The University of New South Wales, Sydney NSW 2052, Australia

SUMMARY

[*]Correspondence: david_sinclair@hms.harvard.edu (D.A.S), leng@mit.edu (L.G.), zarany@mail.med.upenn.edu (Z.A.).
[8]Senior authors
[9]Lead Contact

DECLARATION OF INTERESTS

D.A.S. and L.E.W. are consultants/inventors on patents licensed to Metro International Biotech, Jumpstart Fertility, Life Biosciences, and Liberty Biosecurity and D.A.S. to EdenRoc Sciences, ArcBio, Segterra, Animal Biosciences, Senolytic Therapeutics, Spotlight Biosciences, Continuum Biosciences. L.E.W. is a consultant to Intravital and Jumpstart Fertility. M.S.B. is a consultant to Metro International Biotech. L.P.G. is an advisor to Segterra, Sebelius and Elysium Health. A provisional patent application has been submitted with A.D., L.E.W. and D.A.S. as inventors. The other authors declare no competing interests.

AUTHOR CONTRIBUTIONS

Management, A.D., L.P.G., L.E.W., Z.A., and D.A.S; Experimental design, A.D., G.X.H., Z.A., J.R.M., A.L. and D.A.S.; ESKO, ESTO, pharmacology, A.D., M.S.B., M.B.S., L.J.K., C.L., B.O., S.J., J.H.T., Y.L., M.J.K., N.T.; PGC-1α, G.X.H. and Z.A.; Imaging, A.D., T.H. and B.L.; Resources, A.L., E.O.W., M.I., J.R.M., L.E.W., L.P.G., Z.A. and D.A.S.; Manuscript, rebuttal, revisions, A.D. and D.A.S.; Funding, L.P.G., Z.A., L.E.W. and D.A.S.

A decline in capillary density and blood flow with age is a major cause of mortality and morbidity. Understanding why this occurs is key to future gains in human health. NAD^+ precursors reverse aspects of aging, in part, by activating sirtuin deacylases (SIRT1-7) that mediate the benefits of exercise and dietary restriction (DR). We show that SIRT1 in endothelial cells is a key mediator of pro-angiogenic signals secreted from myocytes. Treatment of mice with the NAD^+ precursor nicotinamide mononucleotide (NMN) improves blood flow and increases endurance in elderly mice by promoting SIRT1-dependent increases in capillary density, an effect augmented by exercise or increasing the levels of hydrogen sulfide (H_2S), a DR mimetic and regulator of endothelial NAD^+ levels. These findings have implications for improving blood flow to organs and tissues, increasing human performance, and reestablishing a virtuous cycle of mobility in the elderly.

Graphical abstract

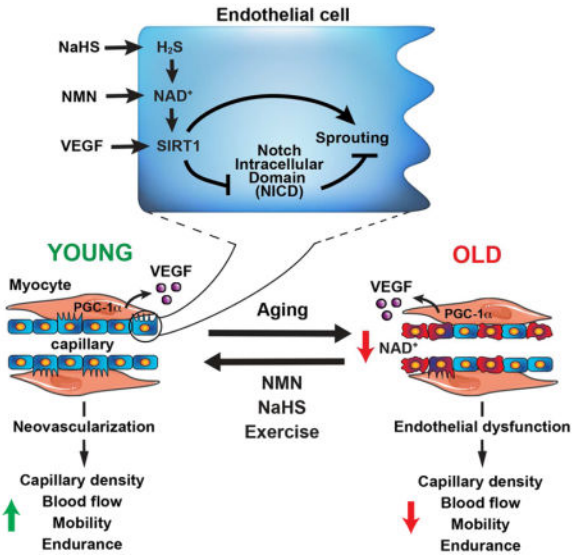

INTRODUCTION

One of the most profound changes to the body as it ages is a decline in the number and function of endothelial cells (ECs) that line the vasculature. The performance of organs and tissues is critically dependent on a functional microcapillary network that maintains a supply of oxygen, exchanges heat and nutrients, and removes waste products (Olfert et al., 2009). According to the Vascular Theory of Aging (Le Couteur and Lakatta, 2010), vascular decline is one of the major causes of aging and age-related diseases.

Despite the importance of capillary loss to human health, it is surprising how little we understand about its underlying causes (Le Couteur and Lakatta, 2010). Exercise is currently the best way to delay the effects of aging on the microvasculature by promoting neovascularization, but little is known about why tissues become desensitized to exercise with age (Bassel-Duby and Olson, 2006; Booth and Thomason, 1991; Hood, 2001). Skeletal muscle is an ideal tissue to study the effects of aging on neovascularization and capillary maintenance. For reasons that are unclear, as we age there is an increase in muscle EC

apoptosis, decreased neovascularization, and blood vessel loss (Groen et al., 2014; Wang et al., 2014), resulting in reduced muscle mass (sarcopenia) and a decline in strength and endurance in the later decades of life, even with exercise (Denis et al., 1986; Prior et al., 2016; Ryan et al., 2006). A few exercise-mimetic agents have been reported that increase mitochondrial function (e.g. resveratrol and PPARδ agonists), none of which are known to work by increasing capillary density or blood flow (Canto et al., 2012; Lagouge et al., 2006; Narkar et al., 2008).

SIRT1 is a member of the sirtuin family of NAD^+-dependent deacylases that mediate the health benefits of DR and can extend lifespan when overexpressed (Guarente, 2013; Haigis and Sinclair, 2010; Kanfi et al., 2012; Satoh et al., 2013). In young muscle, SIRT1 is required for ischemia-induced neovascularization (Potente et al., 2007), vascular relaxation (Mattagajasingh et al., 2007; Pearson et al., 2008; Ungvari et al., 2010) and is implicated in EC senescence (Ota et al., 2007; Zu et al., 2010). It is, however, unknown whether endothelial SIRT1 regulates microvascular remodeling in skeletal muscle tissue, and if so, whether its breakdown with age is cell-autonomous or reversible.

SIRT1 activating compounds (STACs) such as resveratrol and SRT1720 have been pursued as a strategy for ameliorating age-related diseases (Hubbard et al., 2013; Sinclair and Guarente, 2014). A more recent approach has been to restore NAD^+ levels by treating with NAD^+ precursors such as nicotinamide riboside (NR) or nicotinamide mononucleotide (NMN) (Canto et al., 2015; Gomes et al., 2013; Mouchiroud et al., 2013; Ramsey et al., 2008). NAD^+ precursors increase the angiogenic capacity of ECs in cell culture (Borradaile and Pickering, 2009; Hughes-Large et al., 2014), improve the exercise capacity of young mice (Canto et al., 2012), and protect against age-related physiological decline including reduced DNA repair, mitochondrial dysfunction, and glucose intolerance (de Picciotto et al., 2016; Gomes et al., 2013; Li et al., 2017; Yoshino et al., 2011). Whether a decrease in NAD^+ and SIRT1 activity in ECs is a cause of microvasculature loss and frailty during aging is not yet known.

Another DR mimetic is hydrogen sulfide (H_2S), a gas generated endogenously by cystathionine β-synthase (CBS) and/or cystathionine γ-lyase (CSE) (Hine and Mitchell, 2015). Evidence indicates that SIRT1 and H_2S may lie in the same pathway. For example, in *Caenorhabditis elegans*, hydrogen sulfide (H_2S) extends lifespan in a Sir2.1-dependent manner (Miller and Roth, 2007). In mammals, ectopic treatment with H_2S induces SIRT1 in response to oxidative stress (Suo et al., 2013; Wu et al., 2015; Zheng et al., 2014) and protects rat hearts from ischemia/reperfusion via a mechanism requiring SIRT1 (Hu et al., 2016).

In this study, we tested whether a decline in SIRT1 activity in ECs is a major reason why blood flow and endurance decrease with age, and whether SIRT1 stimulation by NMN and/or H_2S can reverse these changes. We show that loss of endothelial SIRT1 results in an early decline in skeletal muscle vascular density and exercise capacity, while overexpression of endothelial SIRT1 has a protective effect, ostensibly by sensitizing ECs to vascular endothelial growth factor (VEGF) coming from muscle fibers. Pharmacologically raising NAD^+ levels promotes muscle vascular remodeling following ischemic injury and restores

capillary density and treadmill endurance of old mice back to youthful levels, and in young mice during chronic exercise, an effect that is further augmented by H_2S.

RESULTS

Aging is associated with decreased muscle microvasculature, endurance and angiogenesis

One of the most reliable, yet pernicious aspects of mammalian aging is a decrease in blood flow to skeletal muscle. Consistent with this, the abundance of ECs and capillaries in skeletal muscle and exercise endurance of 20-month old mice was significantly lower compared to 6-month olds (Fig. 1A–C, S1A).

A possible explanation was impaired angiogenic potential. To test this, a series of *in vitro* angiogenesis assays were performed on mouse lung ECs (MLECs) from young and old mice. MLECs were cultured in the presence of conditioned media (CM) with angiogenic factors provided by peroxisome proliferator-activated receptor γ coactivator 1-α (PGC-1α)–overexpressing C2C12 myotubes (Arany et al., 2008). Compared to young mice, MLECs from 20-month old mice had reduced migratory capacity (Fig. 1D, S1B), decreased ability to form capillary-like structures (Fig. 1E, S1C) and shorter spheroidal sprout lengths (Fig. 1F).

Endothelial SIRT1 deletion mimics the effect of aging on capillary density and endurance

To test if SIRT1 is required for vascular maintenance and angiogenesis late in life, we used a *Tie2-Cre* mouse to knock out or overexpress SIRT1 specifically in the ECs. The EC-specificity of *Tie2* promoter was confirmed using a GFP reporter mouse strain (Fig. 2A, S2A–D). Endothelial-specific SIRT1 knockout mice (ESKO, Fig. 2B–C, S2E–F) were healthy and born in expected Mendelian ratios. In 6-month old ESKO mice, the density and number of capillaries was significantly lower compared to age-matched wildtype (WT) mice (Fig. 2D, S2G).

Although there were no obvious physiological differences between the genotypes (Fig. S2H–J), in a high intensity endurance test ESKO mice ran only half as long and far as their WT littermates (Fig. 2E, Movie 1). There was also a trend towards higher post-exercise serum lactate levels in ESKO mice ($p = 0.055$) (Fig. 2F).

Differences in exercise capacity are commonly attributable to changes in muscle fiber type (Pette and Staron, 2000) or mitochondrial content (Lin et al., 2002). A comparison of gastrocnemius and quadriceps muscles from ESKO and WT mice showed no significant differences in fiber type (Fig. S2K), mitochondrial content (Fig. S2L) or mitochondrial activity (Fig. S2M), further supporting the hypothesis that the low exercise capacity of ESKO mice is due to a reduced number of capillaries.

Endothelial SIRT1 is required for exercise-induced neovascularization

In young individuals, exercise is a potent stimulator of angiogenesis, but this effect wanes considerably with advancing age for reasons that are not known. To test if SIRT1 plays a role in this process, we first subjected 10-month old inducible SIRT1 knockout mice (SIRT1-iKO, Fig. S2N) (Price et al., 2012) to a four-week treadmill training paradigm.

Immediately after SIRT1 deletion, there was no difference in capillary number or density. After four weeks of exercise training, however, the number of capillaries and capillary density in the quadriceps muscle of SIRT1-iKO mice was only 1.4-fold higher compared to 2-fold in WT mice (Fig. 2G), indicating that SIRT1 is required for exercise-induced muscle neovascularization.

PGC-1α increases mitochondrial function and induces the secretion of VEGF to promote neovascularization (Arany et al., 2008). Indeed, mice lacking PGC-1α have limited angiogenesis after exercise (Chinsomboon et al., 2009) whereas mice overexpressing PGC-1α in muscle have increased mitochondria and capillary density (Lin et al., 2002). We deleted SIRT1 either in ECs or myocytes of the muscle-specific PGC-1*α* overexpressing mouse (*MCK-PGC-1α).* Despite there being no effect on mitochondrial protein levels (Fig. S2O–P), *MCK-PGC-1α*;ESKO mice had significantly reduced capillary density compared to *MCK-PGC-1α*;WT mice (Fig. 2H). As shown in Fig. 2I, the presence or absence of SIRT1 in myocytes made no difference in the number of capillaries induced by PGC-1α. Together, these data indicate that SIRT1 in ECs but not myocytes is a critical downstream mediator of PGC-1α-induced signals originating from myofibers. In treadmill tests, *MCK-PGC-1α;*ESKO mice had greatly reduced endurance compared to *MCK-PGC-1α* mice (Fig. 2J) but not in the *MCK-PGC-1α;*MSKO mice (Fig. 2K). Thus, SIRT1 in ECs is required for PGC-1α to improve exercise tolerance, even if mitochondrial function is already higher, underscoring the critical role of the vasculature SIRT1 in endurance.

SIRT1 is required for pro-angiogenic growth factor signaling from myocytes to ECs

To investigate the specific signals that EC SIRT1 responds to, we performed *in vitro* transwell migration and spheroid assays using MLECs derived from WT and ESKO mice. MLECs without SIRT1 had a blunted chemotactic response (Fig. 3A, S3A), reduced tube formation (Fig. 3B), and shorter EC spheroid sprout length (Fig. 3C). Stimulation of EC replication and migration after exercise involves several pro-angiogenic factors including VEGF and basic fibroblast growth factor (FGF) (Arany et al., 2008). To determine if growth factors require SIRT1 activity, we examined aortic rings from WT and SIRT1-iKO mice that were exposed to either VEGF or FGF (Fig. 3D, S3B). Stimulation of spouting was reduced in the aortic rings lacking SIRT1 (Fig. 3D, S3C). SIRT1-deficient human aortic ECs (HAECs) (Fig. S3D) also had a reduced response to growth factors (Fig. 3E, 3F). SIRT1 had no effect on VEGF mRNA or VEGF protein in serum (Fig. S3E, S3F).

Increasing endothelial SIRT1 activity increases muscle capillary density and exercise capacity

Having found that endothelial SIRT1 is necessary for vascular remodeling, we tested if increasing its abundance or activity was sufficient. To test this, an EC-specific SIRT1 overexpressing mouse strain (ESTO, Fig. 4A–B, S4A–B) was generated. There were no apparent physical abnormalities (Fig. S4C–E) or differences in mitochondria (Fig. S4D–H) but interestingly, blood glucose levels were reduced related to WT (Fig. S4I), indicating that endothelial SIRT1 may promote glucose uptake or suppress gluconeogenesis.

Compared to littermate controls, the density and number of capillaries in the quadriceps of ESTO mice was 1.5-fold and 2-fold greater, respectively (Fig. 4C), with similar increases in gastrocnemius (Fig. S4J). Relative to WT, six-month old ESTO mice ran 1.8 times longer and covered 1.9 times the distance before exhaustion (Fig. 4D, Movie 2), and even had lower post-exercise serum lactate (Fig. 4E). Thus, increasing the expression of SIRT1 in ECs is sufficient to increase the capillary density of skeletal muscle and enhance exercise performance.

If endothelial SIRT1 is a downstream mediator of angiogenic signals from myocytes (see Fig. 2 and 3), increasing endothelial SIRT1 should augment these signals. Overexpression of SIRT1 in MLECs increased cell motility (Fig. 4F), tube formation, and sprout length of EC spheroids (Fig. 4G–H). Overexpression of SIRT1 in human umbilical vein ECs (HUVECs) increased the number of branching points by 33% and the total tubule length by 15% compared to the control cells (Fig. 4I, S4K–L). In a spheroid assay, adeno-SIRT1 infected ECs had 19% longer sprout lengths compared to the control cells upon VEGF stimulation (Fig. 4J, S4M). Aortic rings from whole body SIRT1 overexpressing mice (SIRT1-Tg, Fig. S4N) had double the sprout number and triple the total spout area (Fig. 4K). ESTO mice had higher VEGF serum protein levels (Fig. S4O), indicating that SIRT1 is part of a positive feedback pathway sensitizing myocytes to VEGF and is both necessary and sufficient for skeletal muscle capillary formation.

The NAD^+ precursor, NMN, promotes angiogenesis by inhibiting SIRT1-mediated Notch signaling

The loss of exercise responsiveness in older mice might have been due to a decline in SIRT1 or the levels of its co-substrate NAD^+ (Gomes et al., 2013). NAD^+ precursors are an effective way to raise intracellular NAD^+ levels and stimulate SIRT1 activity (Bogan and Brenner, 2008; Gomes et al., 2013; Yoshino et al., 2011). In cell migration, sprouting and tube formation assays (Fig. 5A–D, S5A–D) NMN increased angiogenesis in a SIRT1-dependent manner, significantly improving tubule structure while preventing tube disintegration (Movies 3 and 4). NMN also doubled the number of outgrowths or sprouts from aortic rings taken from 18-month old WT mice but not old SIRT1-iKOs (Fig. 5E, S5E). SIRT3 and SIRT6 also increase the angiogenic potential of ECs in culture (Cardus et al., 2013; Wei et al., 2017). Knockdown of SIRT3 and SIRT6 in HAECs decreased tube formation and spheroid sprouting that was partially rescued by NMN (Fig. S5F–H), indicating that it's angiogenic effects are primarily mediated by SIRT1.

In vertebrates, the Notch signaling pathway is indispensable for blood vessel formation (Blanco and Gerhardt, 2013). Notch signaling in ECs is controlled by the Notch1 intracellular domain (NICD) protein, which in turn is negatively regulated by SIRT1 (Guarani et al., 2011). After stimulation with VEGF or Notch ligand Dll4 (Fig. 5F, S5I), NMN treatment decreased Notch target gene expression and NICD protein levels (Fig. 5G, S5J). Blocking NICD release with the γ-secretase inhibitor DAPT increased sprout length irrespective of SIRT1 levels (Fig. 5H–I, S5K) while treatment with the VEGF receptor inhibitor SU5416 completely blocked sprouting and this was not rescued by NMN treatment (Fig. 5H). NMN treatment induced proliferation (Fig. S5L) and reduced apoptosis in ECs in

a SIRT1-dependent manner, consistent with an inhibition of Notch (Noseda et al., 2004) (Fig. S5M). Thus Notch signaling in ECs depends on NAD^+ levels and the concomitant activity of SIRT1 (Fig. 5J).

NAD^+ reverses loss of the microvasculature and exercise capacity in old mice via SIRT1

During aging, the level of NAD^+ declines in many tissues, in part, due to increased activity of the NAD-consuming enzymes CD38 and PARP1 (Bai et al., 2011b; Camacho-Pereira et al., 2016; Li et al., 2017; Mouchiroud et al., 2013). We hypothesized that decreasing NAD^+ levels in ECs might explain why older individuals have fewer capillaries and decreased blood flow. Gastrocnemius muscle and ECs isolated from 20-month old mice had lower NAD^+ levels compared to those from 6-month olds (Fig. 6A). We reasoned, therefore, that restoring NAD^+ levels in ECs of old mice to youthful levels might also restore capillary density, blood flow, and endurance. To restore NAD^+ levels, we administered NMN to 18-month old mice via drinking water for two months at 400 mg/kg/day (Fig. S6A–C).

NMN restored the number of capillaries and capillary density of the old mice to those typically seen in young mice (Fig. 6B, S6D). Resting muscle perfusion (Fig. 6C, S6E) and soluble oxygen (sO_2) levels were significantly higher in NMN-treated mice compared to controls (Fig. 6D). Mitochondrial protein and activity levels and other muscle properties remained unaltered (Fig. S6F–L). NMN supplementation dramatically increased home-cage oxygen consumption (Fig. S6M) but the most striking effect was a 56–80% improvement in endurance, with lower post-exercise blood lactate (Fig. 6E–F, Movie 5).

To test if SIRT1 is necessary for neovascularization *in vivo*, 20-month old tamoxifen-treated WT and SIRT1-iKO mice were treated with NMN for two months. NMN increased gastrocnemius capillarity in WT but not in the SIRT1-iKO mice (Fig. 6G). Angiogenesis is also important for tissues to recover from ischemia. NMN restored blood volume and capillary density in a SIRT1-dependent manner in mice subjected to femoral artery ligation (Fig. 6H, S6N).

NMN did not alter the capillarity or exercise capacity of sedentary animals younger than 12-months (not shown), consistent with overexpression of Nampt, an NAD biosynthetic gene (Frederick et al., 2015). There was a strong effect, however, in young mice on NMN after endurance training for one month, resulting in 70% more capillaries than untreated sedentary mice, more than twice the effect of NMN alone (Fig. 6I). To test if NMN works by sensitizing ECs to VEGF, we treated mice with axitinib, an inhibitor of VEGF signaling (Fig. S6O) and saw no effect of NMN on capillary density and exercise capacity (Fig. 6J, S6P).

Exogenous hydrogen sulfide activates SIRT1 and augments the effects of NMN

As a signaling molecule, H_2S shares many similarities with NAD^+. It increases SIRT1 activity, protects against oxidative stress and can promote angiogenesis (Longchamp *et al.,* an accompanying submission). Treatment of HUVECs with NaHS or NMN alone increased SIRT1 protein levels but the combination was even more potent (Fig. 7A). NaHS increased intracellular NAD^+ levels, MLECs motility (Fig. 7B–C) and spheroid sprouting (Fig. 7D, S7A), an effect that was SIRT1-dependent (Fig. 7C). Consistent with Longchamp *et al.*, H_2S

increased cell migration independently of VEGF but dependent on SIRT1 (Fig. S7B), while lowering basal OCR while NMN did not (Fig. S7C). These findings indicate that NAD^+ and H_2S have overlapping and distinct functions in ECs.

To test the effects of the NMN-NaHS combination, we co-treated 32-month old mice with NMN and NaHS for four weeks (Fig. S7D). The combination of NaHS and NMN dramatically increased capillary density compared to other treatment groups (Fig. 7E). Neovascularization declines during aging, in part, because of an increase in oxidative stress and EC apoptosis (Dimmeler and Zeiher, 2000; Pearson et al., 2008). In response to H_2O_2 treatment, NMN reduced the number of apoptotic ECs from 42% to 17% and, in combination with NaHS, reduced it to 11% (Fig. 7F, S7E). NMN also reduced apoptosis in HUVECs by 13% and the combination reduced it by 36% (Fig. 7G, S7F). Mice treated with NMN had 1.6-fold increase in time and distance run compared to untreated mice (Fig. 7H), while the combination of NMN with NaHS treatment doubled their endurance.

The reduced baseline capillary density of ESKO mice confounded the interpretation of the effects of NMN and NaHS. To circumvent this, we knocked down SIRT1 in old mice using a lentivirus expressing SIRT1 miRNA downstream of the vascular endothelium cadherin (VE-cad) promoter (Fig. S7G, Table S1) (Zhang et al., 2013). The most efficient miRNA virus was #5, which knocked down SIRT1 80% and raised NICD (Fig. 7I, S7H). SIRT1 was knocked down in 20-month old mice (Fig. 7J, S7I) that were then treated for four weeks with NMN and/or H_2S precursors (NaHS and GYY4137). The ability of NMN alone or in combination with H_2S precursors to increase vascularization was blocked in the SIRT1 knockdown mice (Fig. 7K). Although the system may result in off-target effects and produce short-term effects making it difficult to directly compare them to knockout mice, they are consistent with our previous conclusions that raising NAD^+ levels and stimulating SIRT1 activity in ECs is an effective way to increase angiogenesis and blood flow to improve exercise endurance, a pathway that is further enhanced by co-treatment with H_2S (Fig. S7L).

DISCUSSION

From the age of 40 onward, the tissue perfusion declines steadily and seemingly inexorably, leading to organ dysfunction and increasing frailty in the last decades of life (Degens, 1998; Le Couteur and Lakatta, 2010). Though exercise is recommended, it only delays a cycle of decline, both physically and physiologically (Denis et al., 1986). In this study, we show that a decrease in endothelial NAD^+ is a primary reason why our ability to exercise and receive its benefits diminish as we age. Specifically, endothelial NAD^+ and SIRT1 are critical regulators of vascular remodeling in response to VEGF-stimulated angiogenesis. NMN restores angiogenesis in old mice ostensibly via a SIRT1-reguluated Notch signaling pathway, underscoring the importance of Notch signaling in aging. At 32-months of age, the effects of aging on the mouse microvasculature were surprisingly easy to reverse. As far as we are aware, this is the first time a small molecule has induced neovascularization at an advanced age.

Interestingly, NMN supplementation had no effect on the capillary density of sedentary young to middle-aged mice. Only when coupled with exercise training or after ischemia did

NMN improve these parameters. This result, and the fact that NMN restores the capillary density of elderly mice to youthful levels but not further, indicates that there may be a signal within EC that caps the number of capillaries in muscle that EC NAD^+ can induce, a limit that is overcome by exercise. If this putative factor is found, it could have significant implications for human health. A potential candidate is CBP/p300-interacting transactivator with ED-rich tail 2 (CITED2), an inhibitor of hypoxia-inducible factor 1 (HIF-1α) signaling that is implicated in type 2 diabetes (Wang et al., 2016). It would be interesting to test whether exercise inhibits expression of CITED2 and if NMN requires CITED2 to increase angiogenesis.

Increasing SIRT1 activity has been thought to improve endurance capacity by increasing mitochondrial function (Bai et al., 2011a; Bai et al., 2011b; Baur et al., 2006; Canto et al., 2009; Lagouge et al., 2006; Pearson et al., 2008). Challenging this assumption, there were no changes in the muscle oxidative capacity in ESTO or NMN-treated mice, despite a dramatic increase in endurance. Conversely, increasing muscle oxidative capacity was insufficient to improve endurance in the absence of increased capillarity, indicating the modes by which SIRT1 activators or NAD boosters increase exercise endurance should be reexamined. Although we saw no change in cardiac function or capillary density, we cannot rule out the possibility of cardiac changes.

The ability of NMN to promote angiogenesis raises the question of whether it might stimulate tumor growth. Mice treated with NMN or NR for extended periods show no evidence of increased tumor burden (Mills et al., 2016; Zhang et al., 2016). Indeed, during the course of our studies, no increase in tumor burden was seen with NMN-treatment or in a DEN-induced model of hepatocarcinoma (Fig. S7J–K), though more study is warranted.

A major cause of age-associated endothelial dysfunction is an increase in oxidative stress and apoptosis (Harman, 1956). SIRT1 and H_2S protect against oxidative stress mediated apoptosis and senescence (Miller and Roth, 2007; Salminen et al., 2013; Suo et al., 2013; Wu et al., 2015). We suggest that in response to exercise, a SIRT1-H_2S pathway within ECs prevents apoptosis after oxidative stress and sensitizes the cells to PGC-1α-mediated VEGF secretion (Fig. S7L). During aging, however, NAD^+ levels decline in ECs, leading to a reduction in SIRT1 activity and the ability of ECs to survive oxidative stress and respond to growth factor signaling. The age-associated increase in oxidative stress further reduces SIRT1 expression, exacerbating the decline.

Skeletal muscle isn't the only tissue that requires adequate blood flow to maintain function. Heart, liver, bone and the brain, for example, are critically dependent on blood flow. It will be interesting to test whether upregulation of the endothelial NAD^+-H_2S pathway improves the vasculature and blood flow into those tissues as well. If so, precursors to NAD^+ and H_2S may not only be effective agents for increasing the recovery from vessel blockages and enhancing the effects of exercise, but also for treating the most common of age-related diseases, if not aging itself.

STAR Methods

Contact for Reagent and Resources Sharing

Further information and requests for resources and reagents should be directed to, and will be fulfilled by, the Lead Contact, Dr. David A. Sinclair (david_sinclair@hms.harvard.edu).

Experimental Model and Subject Details

Animals—All experiments were performed according to procedures approved by UNSW Animal Care and Ethics Committee (UNSW, Australia), MIT's Committee on Animal Care (MIT, MA) and Institutional Animal Care and Use Committees (Harvard Medical School, MA). Mice were fed standard chow and housed under a 12 hrs light/12 hrs dark cycle.

The EC specificity of Tie2 promoter was determined by crossing a *Tie2-Cre* mouse to a reporter mouse (*mT-STOP$^{f/f}$-GFP). mT-STOP$^{f/f}$-GFP* mouse expresses membrane-targeted tandem dimer Tomato protein (TOMATO) ubiquitously. When crossed to *Tie2-Cre* mouse (*Tie2-Cre-GFP)* green fluorescent protein (EGFP) is expressed. *Tie2-Cre* mouse was crossed to *SIRT1$^{f/f}$* or *SIRT1^{STOP}* mouse to generate ESKO (*Tie2-Cre;SIRT1$^{f/f}$)* (Cheng et al., 2003; Potente et al., 2007) or ESTO (*Tie2-Cre;SIRT1^{STOP}*) mouse, respectively. *Myog-Cre* was crossed to *SIRT1$^{f/f}$* mouse to generate MSKO mouse. *MCK-PGC-1α* mouse was crossed to ESKO or MSKO mouse where required.

SIRT1-iKO mice were fed tamoxifen (360 mg/kg) diet for five weeks to elicit whole-body SIRT1 exon 4 excision as described previously (Price et al., 2012). In all cases, otherwise indicated, animals were administered NMN (400 mg/kg/day), NaHS (20 mg/kg/day) and/or GYY4137 (20 mg/kg/day) (Rose et al., 2015) via drinking water. NMN stock was changed twice per week and NaHS/GYY4137 was supplemented daily.

Cells—C2C12 and HEK293T cells were grown in DMEM supplemented with 10% FBS and 1% Penicillin/Streptomycin (Pen/Strep) at 37°C with 5% CO_2. ECs (HUVEC, HAEC and MLEC) were cultured in EGM-2 media at 37°C with 3% O_2 and 5% CO_2.

Method Details

Endurance testing of mice—Mice were acclimatized to the treadmill system for 3 days prior to endurance testing by running at 10–15 m/min for 20 min. In low intensity endurance testing, the speed started at 5 m/min for 5 min, and then the speed was increased by 1 every minute until 21 m/min and kept constant. In high intensity endurance testing, the speed started at 13 m/min for 5 min at 5°inclination, and then the speed was increased by 1 every minute until 20 m/min and kept constant for 20 min. Every 20 min, the speed was increased by 5 m/min and held constant for 20 min. In both tests, mice were run until exhaustion. Mice were considered exhausted when they sat on the shocker plate for more than 10 sec without attempting to reinitiate running.

Exercise training of mice—Mice were acclimatized to the treadmill system for 3 days prior to the start of exercise training by running at 10 m/min for 20 min. The animals that were successfully acclimated were then trained at 15–20 m/min at 5°inclination for 30

minutes once daily for 30 days. Mice receiving treatment were given NMN (500 mg/kg/day) and/or axitinib (30 mg/kg/day) throughout the course of exercise training regimen. NMN given via drinking water was changed every 3 days and axitinib (Escudier and Gore, 2011) given via food was changed daily. The exhaustive exercise capacity of the mice was tested at the end of training.

Blood glucose, lactate and VEGF—Mice were fasted for 6 hrs and blood glucose levels were measured by tail bleed using a commercially available glucose meter. Blood lactate was measured before and immediately after treadmill exercise (30 min at 15 m/min) by tail bleed using a commercially available lactate meter. Serum VEGF was measured using a commercially available ELISA kit or by Eve Technologies, Canada.

Urine creatinine—Urine was collected from mice after a 2 hrs fast and analyzed for creatinine levels using a colorimetric assay kit.

Rotarod test—Motor coordination was assessed using the rotarod test as previously described (Mersmann et al., 2011). In short, mice were acclimatized to a rotarod for 3 days in three trials lasting 2 min each at a constant speed of 5 rpm. On the 4^{th} day, the animals were subjected to three trials on the accelerating roller (4 – 40 rpm in 4 min) and the time that the mice remained was recorded.

Hindlimb ischemia—The effect of NMN in ischemia-induced vessel formation was assessed in a murine model of hindlimb ischemia using 8-month old SIRT1-iKO and WT mice according to the published protocol (Limbourg et al., 2009). Treatment of animals with NMN (500 mg/kg/day) via drinking water started one week prior to femoral ligation and was continued until the end of the experiment. The blood flow in the ischemic limb was measured using contrast-enhanced ultrasound imaging, 20 days after the surgery.

Contrast-enhanced ultrasound (CEU)—Mice were anesthetized with isoflurane (1.5–2%, 500 ml O_2/min), hindlimbs were shaved using depilatory cream and a 27-gauge catheter was placed into each mouse's tail and kept in place with surgical tape. Each mouse was placed in a supine position on a platform heated to 38°C with each paw taped to a surface electrode to monitor ECG, heart rate, and respiratory rate. CEU was performed using Vevo 2100 system at an imaging frequency of 18 MHz. The probe was placed on the medial side of the leg to image the lower hindlimb in a sagittal plane. A bolus injection of microbubbles (contrast reagents) were injected through the tail vein catheter according to the manufacturer's instructions. A cine loop was recorded at a frame rate of 20 frames/s for a total of 1,000 frames. Curve fit analysis was used to measure echo power over time. The difference in maximum and minimum video intensity was determined as the peak enhancement (Baltgalvis et al., 2014).

Cardiac ultrasound—Parasternal short-axis M-mode images were acquired using the Vevo 2100 system as previously described (Respress and Wehrens, 2010). Mice were anesthetized with 1–2% isoflurane, and heart rate was measured between 450 and 500 beats/min.

Photoacoustic imaging—Mice were anesthetized with isoflurane (1.5–2%, 500 ml O_2/min), and body portion below chest area was shaved using depilatory cream. The animals were then placed horizontally in the imaging chamber of MSOT inVision 256-TF small animal imaging system and three-dimensional scanning of the lower portion was performed as per manufacture's protocol (Morscher et al., 2014).. Briefly, a tunable optical parametric oscillator (OPO) pumped by an Nd:YAG laser provided excitation pulses with a duration of 9 ns at wavelengths from 680 nm to 980 nm at a repetition rate of 10 Hz with a wavelength tuning speed of 10 ms and a peak pulse energy of 100 mJ at 730 nm. Ten arms of a fiber bundle provided even illumination of a ring-shaped light strip of approx. 8 mm width. For ultrasound detection, 256 toroidally focused ultrasound transducers with a center frequency of 5 MHz (60% bandwidth), organized in a concave array of 270° an gular coverage and a radius of curvature of 4 cm, were used.

Metabolic measurements and body composition—Metabolic chambers were used to perform whole-body measurements of metabolic function. Following acclimatization to the metabolic chambers, individually housed mice were monitored continuously over 48 hrs to determine oxygen consumption, carbon dioxide production, respiratory exchange ratio, energy expenditure, food intake, water intake and activity. Body composition (fat mass, lean mass, and total body water) was measured by EchoMRI.

Permeabilized fiber respiration—Permeabilized fibres were prepared and mitochondrial function was analyzed according to published protocols with some modifications (Kuznetsov et al., 2008). Briefly, soleus and extensor digitorum longus (EDL) muscles were dissected tendon-to-tendon into ice-cold isolation buffer A and fibers were prepared immediately. Fiber bundles (~3 mg wet weight) were treated with saponin (50 μg/mL) for 20 min at 4°C and subsequently washed in cold respiration medium B (0.5 mM EGTA, 3 mM $MgCl_2.6H_2O$, 20 mM taurine, 10 mM KH_2PO_4, 20 mM HEPES, 0.1% BSA, 15 mM potassium-lactobionate, 110 mM mannitol, 0.3 mM dithiothreitol, pH 7.1). Mitochondrial respiratory chain function was analyzed on a Clark-type electrode *in situ* in respiration medium B at 37°C with the sequential addition of glutamate (10 mM), malate (5 mM), ADP (2 mM), rotenone (0.5 μM), succinate (10 mM), antimycin A (5 μM), *N,N,N′,N′*-tetramethyl-*p*-phenylenediamine dihydrochloride (0.5 mM TMPD) and ascorbate (2 mM), cytochrome *c* (10 μM). Fibers were recovered after polarography and results were expressed as nmoles of O_2/min/mg of tissue. Mitochondrial membrane integrity was verified by cytochrome *c* release test.

Enzyme activity assays—Quadriceps muscle was homogenized 1:19 (w/v) in 50 mM Tris-HCl, 1 mM EDTA, 0.1% Triton X-100, pH 7.4. The homogenates were subjected to three freeze-thaw cycles and centrifuged for 10 min at 7,000 × g at 4°C. Supernatants were used to determine the activity for citrate synthase (CS) and succinate dehydrogenase (SDH) as described previously (Turner et al., 2009). Cytochrome c oxidase staining of muscle sections was performed according to the published protocol (Ross, 2011). Briefly, 20 μm cryostat sections of quadriceps muscle were incubated with Cytochrome *c* (0.1 mM), catalase (2 μg/mL) and DAB (0.05%) in PBS for 40 min at 37°C. The slides were

dehydrated through alcohol, cleared in xylene and then mounted with DPX. The slides were images using Aperio XT Slide Scanner.

NAD^+ measurements—Levels of NAD^+ in ECs and muscle homogenates were measured using commercially available kit. Alternatively, NAD^+ levels in muscle and liver were measured by assay in-house developed method (Uddin et al., 2016). In brief, liver and gastrocnemius samples were homogenized in extraction buffer (10 mM Tris-HCl, 0.5% TritonX-100, 10 mM Nicotinamide, pH7.4) and then centrifuged (12,000 × g for 5 min at 4°C), after which an aliquot of supernatan t was taken for protein quantification. After phenol:chloroform:isoamylalcohol (25:24:1) and chloroform extractions the supernatant was separated in two aliquots. One was used to measure total NAD. The other aliquot was acidified with HCl, and then neutralized with NaOH on ice to quantify NAD^+. Samples were mixed in a 96-well plate samples were mixed with alcohol dehydrogenase at room temperature. Total NADH and NAD^+ were quantified using a plate reader.

Genotyping PCR analysis—Small piece of tail or tissue obtained from SIRT1-iKO and WT was incubated in 50 μL of alkaline lysis reagent (25 mM NaOH, 0.2 mM EDTA, pH 12) and incubated at 100°C for 1 hr. After cooling, 50 μL of neutralizing reagent (40 mM Tris-HCl, pH 5) was added and 2 μL of the supernatant was used for PCR to detect the excision of SIRT1 gene using the primers Sir2A6860 and Sir2A6171.

Primary mouse EC (MLEC) isolation—MLECs from lungs and muscles were isolated and purified according to published protocol (van Beijnum et al., 2008) with some modifications. Briefly, tissues were collected, weighed, rinsed with cold PBS, minced with sterile blades and then washed with DMEM media (10% FBS and 1% Pen/Strep). After adding 2.5 mL of digestion buffer (1 mg/mL Collagenase/Dispase, 0.1 mg/mL DnaseI in DMEM) per 100 mg of tissue, the mixture was incubated at 37°C for 20 min with shaking in a gentleMACS dissociator. The resulting suspension was then filtered through a 100-μ filter into an equal volume of washing/blocking buffer (20% FBS in PBS). The flow-through was spun at 300 × g for 5 min, supernatant discarded and the cells were suspended in 10 mL of washing/blocking buffer. The solution was filtered through 70-μ filter, spun again, resuspended in 2 mL RBC lysis buffer (155 mM NH_4Cl, 12 mM $NaHCO_3$ and 0.1 mM EDTA) and incubated for 5 min at room temperature. Immediately afterwards, 10x volume of washing/blocking buffer was added and the solution was filtered through a 40-μ filter. The cells were collected by centrifugation, resuspended in Antibody Binding Buffer (2 mM EDTA, 1% FBS, 0.5% BSA and 2mM EDTA in PBS) and counted. MLECs were then isolated using CD31-APC antibody and EasySep mouse APC positive selection kit according to manufacturer's instructions. MLECs were cultured as described before.

Measurement of percent skeletal muscle ECs—Skeletal muscles from the hindlimbs were isolated, then digested with collagenase/dispase as described before and filtered through a 40-μ filter. The number of cells was counted and the cell suspension was incubated with APC-conjugated anti-mouse CD31 antibody for 20 min. Number of $CD31^+$ ECs were measured and analyzed by flow cytometry.

RNA interference and viral infection—ECs were transfected with ON-Target*plus* SMART pool siRNA reagents using Dharmafect 4 transfection reagent as per manufacturer's protocol. ON-TARGET*plus* Non-Targeting pool siRNA (NT) was used as a negative control. SIRT1 silencing was also achieved using pLKO.1 lentiviral plasmid mediated shRNA expression according to the published protocol (http://www.addgene.org/tools/protocols/plko/). Briefly, psPAX2, pMD2.G and lentiviral vector plasmids were co-transfected into 293T cells using FuGENE HD transfection reagent. At 48 hrs post-transfection, virus was harvested and ECs were infected. pLKO.1 encoding a scrambled shRNA (Scr) was used as a negative control. ECs were infected with adenoviruses expressing human SIRT1 or GFP according to manufacturer's protocol. ECs were used for different angiogenesis assays, 24 hours post-transfection/infection.

Dll4 and VEGF stimulation of ECs—The ECs to be stimulated were serum-staved overnight and transferred to media containing VEGF (50 ng/mL) or to Dll4-coated plates, and then incubated for indicated time. Dll4 coating was performed as described before (Guarani et al., 2011). Dll4 were reconstituted in PBS containing 0.1% bovine serum albumin (BSA). The culture dishes were coated with Dll4 (0.5 μg/mL) in 0.1% gelatin solution for 1 hr at 37°C. ECs were pre-incubated with NMN (0.5 mM) overnight prior to stimulation wherever indicated.

Construction of miRNA vectors and lentivirus production—The lentivirus plasmids expressing different miRNAs were constructed according to the published method (Zhang et al., 2013). Pre-miRNA sequences targeting mouse SIRT1 open reading frame (GenBank accession no. NM_019812.3) were designed using the BLOCK-iT RNAi designer tool. Oligos corresponding to miRNAs (Table S1) were annealed and ligated into pcDNA6.2-GW/EmGFP-miR vector according to manufacturer's instructions. pcDNA6.2-GW/EmGFP-miR-neg control plasmid was used as a control. The fragments carrying EmGFP and miRNA sequences were amplified by polymerase chain reaction (PCR) using the primers: sense, 5′-AGGCGCGCCTGGCTAACTAGAGAAC-3′, and antisense, 5′-GAATTCTATCTCGAGTGCGGC-3′. The amplified fragments were digested with *AscI* and *EcoRI*, and then inserted into the *AscI* and *EcoRI* sites of Lenti-VE-Cad miRNA plasmid to generate lentiviral plasmids expressing NT or SIRT1 miRNAs (#1–4). Lentiviral particles were produced as described before and concentrated in PBS by ultracentrifugation to ~1×10^{12} transducing units (TU)/mL. The lentiviral titer was measured using a qRT-PCR titration kit according to the manufacturer's instructions.

MLECs were infected with lentiviral particles at a multiplicity of infection (MOI) of 30. Lentiviral particles (1×10^{10} TU) were injected to animals via retro-orbital injection. Mice received two consecutive injections behind alternate eyes two days apart. 10 days post final injection; mice were assigned to different treatment groups. Cells/mice expressing SIRT1 miRNA #5 was generated by co-infecting equal titers of lentiviral particles carrying SIRT1 miRNA #1 and #4.

C2C12 Conditioned Media (CM)—C2C12 myoblasts transfected with adenovirus expressing PGC-1α were differentiated in DMEM supplemented with 5% heat inactivated

horse and then conditioned media (CM) was collected by replacing the differentiation medium with DMEM (1% FBS) medium for 48 hrs.

Transwell migration assay—Chemotaxis assays were performed as described previously (Oommen et al., 2011). Primary murine lung endothelial cells (MLECs) were serum-starved overnight and then seeded ($2.5 – 5 \times 10^4$ cells) in the upper compartment of a transwell. C2C12 CM or DMEM was added to the bottom well to serve as chemo-attractant for MLECs. HUEVCs and HAECs were stimulated with EBM-2 media (0.2% FBS) containing VEGF (50 ng/mL) or FGF (50 ng/mL). NMN (0.5 mM) and/or NaHS (0.1 mM) were added to the chemo-attractant media wherever mentioned. ECs were allowed to migrate for 24 hrs, after which cells were fixed, stained with DAPI and quantified by Fiji software. For each biological replicates (see figure legend) at least three random fields were photographed (@10X, Nikon Eclipse T*i*).

Tube formation assay—Formation of tube networks was assessed as described before (Borradaile and Pickering, 2009). ECs were seeded at 10,000 cells per well in a 24-well plate coated with 150 μL Cultrex reduced growth factor basement membrane matrix. The cells were simulated with C2C12 CM or EBM-2 medium containing VEGF (30 ng/mL) or FGF (30 ng/mL). NMN (0.5 mM) and NaHS (0.1 mM) were added to the media wherever mentioned. Following an 18 hrs-incubation, resulting tube networks from each biological replicates (see figure legend) were analyzed in at least three random fields by light microscopy (@10X, Nikon Eclipse TiE). The number of branch points and total length of tubule networks were quantified by Fiji software (Angiogenesis Analyzer).

Spheroid assay—EC spheroids were generated as described previously (Korff and Augustin, 1998). Briefly, ECs (1000 cells per spheroid) were suspended in EGM-2 medium containing 20% methocel and seeded in non-adherent round-bottom 96-well plates. Under these conditions all suspended cells contributed to the formation of a single spheroid. The spheroids were harvested after 24 hrs and embedded into 400 μL of 2.2 mg/mL collagen gels. Sprouting was initiated by adding 200 μL of C2C12 CM or EBM-2 medium containing VEGF (50 ng/mL). DMEM (1% FBS) or EBM-2 (BSA) was used as control for C2C12 CM or EBM-2 (VEGF), respectively. NMN (0.5 mM), NaHS (0.1 mM), DAPT (20 μM) or SU5416 (10 μM) were added to the media wherever mentioned. After 24 hrs, spheroids were photographed using phase-contrast microscopy (@10X, Nikon Eclipse T*i*) and angiogenic capacity was quantified by measuring the sprout length that had grown out of each spheroid analyzing 8–10 spheroids per group. DAPT: γ-secretase inhibitor, SU5416: VEGFR2 inhibitor.

Aortic ring assay—Aortic ring assay was performed according to the published protocol (Baker et al., 2012). Briefly, thoracic aortas from mice were excised, cut into ~0.5 mm wide rings and serum starved overnight by incubating in Opti-MEM medium (1% Pen/Strep). Next day, each aortic ring was embedded in 50 μL of 1 mg/mL collagen matrix in a 96-well plate and vessel sprouting was stimulated by supplementing with VEGF (30 ng/mL) or FGF (30 ng/mL) in 150 μL of Opti-MEM culture containing FBS (2.5%). Control condition was minimal growth factors (2.5% FBS) with almost no sprouting because of low factor

stimulation, as reported elsewhere (Baker et al., 2012). NMN (0.5 mM) or DAPT (20 μM) were added to the media wherever mentioned. The media was replaced every two days. After incubating for 7 days, the resulting sprouts were stained with BS1 lectin-FITC and imaged using fluorescence microscope (@4X, Nikon A1). The number and total area of sprouts originating from aortic rings were quantified by Fiji software. Aortic rings were collected from at least 8 mice per experiment (see figure legend) and assay was performed using 4–5 technical replicates.

Wound scratch assay—ECs were cultured in a 24-well plate until forming a confluent monolayer and a scratch was made using a 200 μL pipette tip. ECs were allowed to migrate ± NaHS (0.1 mM) and ± NMN (0.5 mM) in EGM-2 medium for 6 hrs. Images were taken at the same location using a brightfield inverted microscope (Olympus 2467) every 2 hrs. The area of gap closure was calculated using Fiji software.

Proliferation assay—ECs (0.1×10^5 cells) were seeded in a 48-well plate and incubated ± NMN (0.5 mM) in EGM-2 medium for 48 hrs. At the end of the incubation time, cell number was determined using flow cytometry.

Apoptosis assay—HUVECs were pretreated ± NaHS (0.1 mM), ± NMN (0.5 mM) for 6 hrs, followed by exposure to H_2O_2 (0.6 mM) for another 4 hrs. After treatments, the number of apoptotic cells was determined using Annexin V-FITC apoptosis detection kit as per manufacturer's instruction. Annexin-V and PI staining were detected with a flow cytometry. MLECs were serum starved overnight ± NMN (0.5 mM) and the number of apoptotic cells was determined as above.

Seahorse analysis—Oxygen consumption rates (OCR) were measured using Seahorse XF96 analyzer. Briefly, 40,000 HUVECs were plated onto XF96 plates and incubated overnight at 37°C/5% CO_2. Next day, the media was replaced with XF assay media (DMEM, 1 g/L glucose, 2 mM glutamate, 1mM pyruvate, pH 7.4). NaHS (0.1 mM) and/or NMN (0.5 mM) were added at the start of the experiment. OCR measurements were made approximately every 8 min under basal conditions, and after the addition of oligomycin (1 μM). Experiments were replicated in six wells and averaged for each experimental condition.

Immunofluorescence—Freshly isolated whole quadriceps and gastrocnemius muscle samples were mounted in O.C.T. compound, placed in an isopentane bath and slowly cooled in liquid nitrogen. Transverse sections at 20 μm-thickness were sectioned on a cryostat. The sections were fixed in pre-cooled acetone (−20°C) for 10 min. In case of cells, 4% paraformaldehyde in TBS (50 mM Tric-HCl, 150 mM NaCl, pH7.5) was used for fixation. The slides were washed with TBS twice and the tissues/cells were permeabilized by incubating with TBST (TBS + 0.1% Triton-X) for 10 min at room temperature. The slides were washed with TBS twice, blocked with BlockAid blocking solution for 1 h at room temperature, and then incubated with primary antibodies diluted in blocking buffer (1:100) overnight at 4°C. Next day, slides were washed with PBS and incubated with secondary antibodies (1:500 dilution) for 2 h at room temperature. Slides were washed again with TBS and mounted with mounting medium. Images were acquired using a confocal fluorescence

microscope (Nikon A1). Muscle cross-sections were immunostained with anti-CD31 and anti-laminin antibodies to visualize capillaries and basal lamina surrounding the fibers, respectively. We restricted our examination to the mid-portion of the muscles because of its high capillary density and well-known adaptations to exercise (Chinsomboon et al., 2009). Quantification of capillaries and capillary density were performed using Fiji software. TUNEL staining was performed in muscle sections using TUNEL assay kit as per manufacturer's protocol.

Hematoxylin and eosin (H&E) staining—After fixation of frozen sections, samples were stained with 0.1% Hematoxylin for 10 min, rinsed with dH_2O, stained with Scott's blue solution for 1 min and then washed with dH_2O. The sections were then dipped in Eosin for 3 min, dehydrated through alcohol and cleared in xylene. The slides were mounted with DPX and imaged using Aperio XT Slide Scanner.

RNA analysis—Total mRNA was isolated from cells and tissues using TRIzol. cDNAs were synthesized from 1 μg of total RNA using iScript Reverse Transcription Supermix. qPCR was performed with LightCycler 48 SYBR Green I Mastermix using the LightCycler 480 System according to the manufacturer's instructions. Relative mRNA expression levels were calculated using the ΔΔCt method. The forward and reverse primer sequences used in qPCR amplification reactions are displayed in Table S2.

Western—SDS-PAGE and Western blot analysis was performed according to standard procedures and detected with the ECL detection kit. Quantification of band intensities by densitometry was carried out using Fiji software.

Quantification and Statistical Analysis

Data are presented as means ± SEM. Statistical significance was performed using Student's t test, one-way or two-way ANOVA with Bonferroni's Multiple Comparisons Test. Statistical test was performed using GraphPad Prism software. P values of less than 0.05 were considered statistically significant.

Supplementary Material

Refer to Web version on PubMed Central for supplementary material.

Acknowledgments

We thank Margaret Morris, Edna Hardeman, Doyle Lokitiyakul, Anthony Kee, Kyle Hoehn, Corrine Fiveash, Ellen Olzomer, Menghan Liu, Patty Lee, Yi Zhang, Neil Youngson, Golam Mezbah Uddin, Nicholas Bentley, BMIF-BRIL-BRC (UNSW) and Paul Glenn for support. Supported by the Glenn Foundation for Medical Research, RO1 AG028730 and RO1 DK100263, the Sinclair Gift Fund, a gift from Edward Schulak to D.A.S., NIH/NIA RO1 AG015339 to L.P.G. and NIH/NHLBI award RO1 HL094499 to Z.A. This study is dedicated to Vera Ryan, grandmother to D.A.S., who believed the measure of a person is not their status or wealth but their impact.

References

Arany Z, Foo SY, Ma Y, Ruas JL, Bommi-Reddy A, Girnun G, Cooper M, Laznik D, Chinsomboon J, Rangwala SM, et al. HIF-independent regulation of VEGF and angiogenesis by the transcriptional coactivator PGC-1alpha. Nature. 2008; 451:1008–1012. [PubMed: 18288196]

Bai P, Canto C, Brunyanszki A, Huber A, Szanto M, Cen Y, Yamamoto H, Houten SM, Kiss B, Oudart H, et al. PARP-2 regulates SIRT1 expression and whole-body energy expenditure. Cell Metab. 2011a; 13:450–460. [PubMed: 21459329]

Bai P, Canto C, Oudart H, Brunyanszki A, Cen Y, Thomas C, Yamamoto H, Huber A, Kiss B, Houtkooper RH, et al. PARP-1 inhibition increases mitochondrial metabolism through SIRT1 activation. Cell Metab. 2011b; 13:461–468. [PubMed: 21459330]

Baker M, Robinson SD, Lechertier T, Barber PR, Tavora B, D'Amico G, Jones DT, Vojnovic B, Hodivala-Dilke K. Use of the mouse aortic ring assay to study angiogenesis. Nat Protoc. 2012; 7:89–104.

Baltgalvis KA, White K, Li W, Claypool MD, Lang W, Alcantara R, Singh BK, Friera AM, McLaughlin J, Hansen D, et al. Exercise performance and peripheral vascular insufficiency improve with AMPK activation in high-fat diet-fed mice. Am J Physiol Heart Circ Physiol. 2014; 306:H1128–1145. [PubMed: 24561866]

Bassel-Duby R, Olson EN. Signaling pathways in skeletal muscle remodeling. Annu Rev Biochem. 2006; 75:19–37. [PubMed: 16756483]

Baur JA, Pearson KJ, Price NL, Jamieson HA, Lerin C, Kalra A, Prabhu VV, Allard JS, Lopez-Lluch G, Lewis K, et al. Resveratrol improves health and survival of mice on a high-calorie diet. Nature. 2006; 444:337–342. [PubMed: 17086191]

Blanco R, Gerhardt H. VEGF and Notch in tip and stalk cell selection. Cold Spring Harb Perspect Med. 2013; 3:a006569. [PubMed: 23085847]

Bogan KL, Brenner C. Nicotinic acid, nicotinamide, and nicotinamide riboside: a molecular evaluation of NAD+ precursor vitamins in human nutrition. Annu Rev Nutr. 2008; 28:115–130. [PubMed: 18429699]

Booth FW, Thomason DB. Molecular and cellular adaptation of muscle in response to exercise: perspectives of various models. Physiol Rev. 1991; 71:541–585. [PubMed: 2006222]

Borradaile NM, Pickering JG. Nicotinamide phosphoribosyltransferase imparts human endothelial cells with extended replicative lifespan and enhanced angiogenic capacity in a high glucose environment. Aging Cell. 2009; 8:100–112. [PubMed: 19302375]

Camacho-Pereira J, Tarrago MG, Chini CCS, Nin V, Escande C, Warner GM, Puranik AS, Schoon RA, Reid JM, Galina A, et al. CD38 Dictates Age-Related NAD Decline and Mitochondrial Dysfunction through an SIRT3-Dependent Mechanism. Cell Metab. 2016; 23:1127–1139. [PubMed: 27304511]

Canto C, Gerhart-Hines Z, Feige JN, Lagouge M, Noriega L, Milne JC, Elliott PJ, Puigserver P, Auwerx J. AMPK regulates energy expenditure by modulating NAD+ metabolism and SIRT1 activity. Nature. 2009; 458:1056–1060. [PubMed: 19262508]

Canto C, Houtkooper RH, Pirinen E, Youn DY, Oosterveer MH, Cen Y, Fernandez-Marcos PJ, Yamamoto H, Andreux PA, Cettour-Rose P, et al. The NAD(+) precursor nicotinamide riboside enhances oxidative metabolism and protects against high-fat diet-induced obesity. Cell Metab. 2012; 15:838–847. [PubMed: 22682224]

Canto C, Menzies KJ, Auwerx J. NAD(+) Metabolism and the Control of Energy Homeostasis: A Balancing Act between Mitochondria and the Nucleus. Cell Metab. 2015; 22:31–53. [PubMed: 26118927]

Cardus A, Uryga AK, Walters G, Erusalimsky JD. SIRT6 protects human endothelial cells from DNA damage, telomere dysfunction, and senescence. Cardiovasc Res. 2013; 97:571–579. [PubMed: 23201774]

Cheng HL, Mostoslavsky R, Saito S, Manis JP, Gu Y, Patel P, Bronson R, Appella E, Alt FW, Chua KF. Developmental defects and p53 hyperacetylation in Sir2 homolog (SIRT1)-deficient mice. Proc Natl Acad Sci U S A. 2003; 100:10794–10799. [PubMed: 12960381]

Chinsomboon J, Ruas J, Gupta RK, Thom R, Shoag J, Rowe GC, Sawada N, Raghuram S, Arany Z. The transcriptional coactivator PGC-1alpha mediates exercise-induced angiogenesis in skeletal muscle. Proc Natl Acad Sci U S A. 2009; 106:21401–21406. [PubMed: 19966219]

de Picciotto NE, Gano LB, Johnson LC, Martens CR, Sindler AL, Mills KF, Imai S, Seals DR. Nicotinamide mononucleotide supplementation reverses vascular dysfunction and oxidative stress with aging in mice. Aging Cell. 2016; 15:522–530. [PubMed: 26970090]

Degens H. Age-related changes in the microcirculation of skeletal muscle. Adv Exp Med Biol. 1998; 454:343–348. [PubMed: 9889909]

Denis C, Chatard JC, Dormois D, Linossier MT, Geyssant A, Lacour JR. Effects of endurance training on capillary supply of human skeletal muscle on two age groups (20 and 60 years). J Physiol (Paris). 1986; 81:379–383. [PubMed: 3572830]

Dimmeler S, Zeiher AM. Endothelial cell apoptosis in angiogenesis and vessel regression. Circ Res. 2000; 87:434–439. [PubMed: 10988233]

Escudier B, Gore M. Axitinib for the management of metastatic renal cell carcinoma. Drugs R D. 2011; 11:113–126. [PubMed: 21679004]

Firestein R, Blander G, Michan S, Oberdoerffer P, Ogino S, Campbell J, Bhimavarapu A, Luikenhuis S, de Cabo R, Fuchs C, et al. The SIRT1 deacetylase suppresses intestinal tumorigenesis and colon cancer growth. PLoS One. 2008; 3:e2020. [PubMed: 18414679]

Frederick DW, Davis JG, Davila A Jr, Agarwal B, Michan S, Puchowicz MA, Nakamaru-Ogiso E, Baur JA. Increasing NAD synthesis in muscle via nicotinamide phosphoribosyltransferase is not sufficient to promote oxidative metabolism. J Biol Chem. 2015; 290:1546–1558. [PubMed: 25411251]

Gomes AP, Price NL, Ling AJ, Moslehi JJ, Montgomery MK, Rajman L, White JP, Teodoro JS, Wrann CD, Hubbard BP, et al. Declining NAD(+) induces a pseudohypoxic state disrupting nuclear-mitochondrial communication during aging. Cell. 2013; 155:1624–1638. [PubMed: 24360282]

Groen BB, Hamer HM, Snijders T, van Kranenburg J, Frijns D, Vink H, van Loon LJ. Skeletal muscle capillary density and microvascular function are compromised with aging and type 2 diabetes. J Appl Physiol (1985). 2014; 116:998–1005. [PubMed: 24577061]

Guarani V, Deflorian G, Franco CA, Kruger M, Phng LK, Bentley K, Toussaint L, Dequiedt F, Mostoslavsky R, Schmidt MH, et al. Acetylation-dependent regulation of endothelial Notch signalling by the SIRT1 deacetylase. Nature. 2011; 473:234–238. [PubMed: 21499261]

Guarente L. Calorie restriction and sirtuins revisited. Genes Dev. 2013; 27:2072–2085. [PubMed: 24115767]

Haigis MC, Sinclair DA. Mammalian sirtuins: biological insights and disease relevance. Annu Rev Pathol. 2010; 5:253–295. [PubMed: 20078221]

Harman D. Aging: a theory based on free radical and radiation chemistry. J Gerontol. 1956; 11:298–300. [PubMed: 13332224]

Hine C, Mitchell JR. Calorie restriction and methionine restriction in control of endogenous hydrogen sulfide production by the transsulfuration pathway. Exp Gerontol. 2015; 68:26–32. [PubMed: 25523462]

Hood DA. Invited Review: contractile activity-induced mitochondrial biogenesis in skeletal muscle. J Appl Physiol (1985). 2001; 90:1137–1157. [PubMed: 11181630]

Hu MZ, Zhou B, Mao HY, Sheng Q, Du B, Chen JL, Pang QF, Ji Y. Exogenous Hydrogen Sulfide Postconditioning Protects Isolated Rat Hearts From Ischemia/Reperfusion Injury Through Sirt1/PGC-1alpha Signaling Pathway. Int Heart J. 2016

Hubbard BP, Gomes AP, Dai H, Li J, Case AW, Considine T, Riera TV, Lee JE, ESY, Lamming DW, et al. Evidence for a common mechanism of SIRT1 regulation by allosteric activators. Science. 2013; 339:1216–1219. [PubMed: 23471411]

Hughes-Large JM, Pang DK, Robson DL, Chan P, Toma J, Borradaile NM. Niacin receptor activation improves human microvascular endothelial cell angiogenic function during lipotoxicity. Atherosclerosis. 2014; 237:696–704. [PubMed: 25463108]

Kanfi Y, Naiman S, Amir G, Peshti V, Zinman G, Nahum L, Bar-Joseph Z, Cohen HY. The sirtuin SIRT6 regulates lifespan in male mice. Nature. 2012; 483:218–221. [PubMed: 22367546]

Korff T, Augustin HG. Integration of endothelial cells in multicellular spheroids prevents apoptosis and induces differentiation. J Cell Biol. 1998; 143:1341–1352. [PubMed: 9832561]

Kuznetsov AV, Veksler V, Gellerich FN, Saks V, Margreiter R, Kunz WS. Analysis of mitochondrial function in situ in permeabilized muscle fibers, tissues and cells. Nat Protoc. 2008; 3:965–976. [PubMed: 18536644]

Lagouge M, Argmann C, Gerhart-Hines Z, Meziane H, Lerin C, Daussin F, Messadeq N, Milne J, Lambert P, Elliott P, et al. Resveratrol improves mitochondrial function and protects against

metabolic disease by activating SIRT1 and PGC-1alpha. Cell. 2006; 127:1109–1122. [PubMed: 17112576]

Le Couteur DG, Lakatta EG. A vascular theory of aging. J Gerontol A Biol Sci Med Sci. 2010; 65:1025–1027. [PubMed: 20650862]

Li J, Bonkowski MS, Moniot S, Zhang D, Hubbard BP, Ling AJ, Rajman LA, Qin B, Lou Z, Gorbunova V, et al. A conserved NAD+ binding pocket that regulates protein-protein interactions during aging. Science. 2017; 355:1312–1317. [PubMed: 28336669]

Li S, Czubryt MP, McAnally J, Bassel-Duby R, Richardson JA, Wiebel FF, Nordheim A, Olson EN. Requirement for serum response factor for skeletal muscle growth and maturation revealed by tissue-specific gene deletion in mice. Proc Natl Acad Sci U S A. 2005; 102:1082–1087. [PubMed: 15647354]

Limbourg A, Korff T, Napp LC, Schaper W, Drexler H, Limbourg FP. Evaluation of postnatal arteriogenesis and angiogenesis in a mouse model of hind-limb ischemia. Nat Protoc. 2009; 4:1737–1746. [PubMed: 19893509]

Lin J, Wu H, Tarr PT, Zhang CY, Wu Z, Boss O, Michael LF, Puigserver P, Isotani E, Olson EN, et al. Transcriptional co-activator PGC-1 alpha drives the formation of slow-twitch muscle fibres. Nature. 2002; 418:797–801. [PubMed: 12181572]

Mattagajasingh I, Kim CS, Naqvi A, Yamamori T, Hoffman TA, Jung SB, DeRicco J, Kasuno K, Irani K. SIRT1 promotes endothelium-dependent vascular relaxation by activating endothelial nitric oxide synthase. Proc Natl Acad Sci U S A. 2007; 104:14855–14860. [PubMed: 17785417]

Mersmann N, Tkachev D, Jelinek R, Roth PT, Mobius W, Ruhwedel T, Ruhle S, Weber-Fahr W, Sartorius A, Klugmann M. Aspartoacylase-lacZ knockin mice: an engineered model of Canavan disease. Plos One. 2011; 6:e20336. [PubMed: 21625469]

Miller DL, Roth MB. Hydrogen sulfide increases thermotolerance and lifespan in Caenorhabditis elegans. Proc Natl Acad Sci U S A. 2007; 104:20618–20622. [PubMed: 18077331]

Mills KF, Yoshida S, Stein LR, Grozio A, Kubota S, Sasaki Y, Redpath P, Migaud ME, Apte RS, Uchida K, et al. Long-Term Administration of Nicotinamide Mononucleotide Mitigates Age-Associated Physiological Decline in Mice. Cell Metab. 2016; 24:795–806. [PubMed: 28068222]

Morscher S, Driessen WH, Claussen J, Burton NC. Semi-quantitative Multispectral Optoacoustic Tomography (MSOT) for volumetric PK imaging of gastric emptying. Photoacoustics. 2014; 2:103–110. [PubMed: 25431754]

Mouchiroud L, Houtkooper RH, Auwerx J. NAD(+) metabolism: a therapeutic target for age-related metabolic disease. Crit Rev Biochem Mol Biol. 2013; 48:397–408. [PubMed: 23742622]

Narkar VA, Downes M, Yu RT, Embler E, Wang YX, Banayo E, Mihaylova MM, Nelson MC, Zou Y, Juguilon H, et al. AMPK and PPARdelta agonists are exercise mimetics. Cell. 2008; 134:405–415. [PubMed: 18674809]

Noseda M, Chang L, McLean G, Grim JE, Clurman BE, Smith LL, Karsan A. Notch activation induces endothelial cell cycle arrest and participates in contact inhibition: role of p21Cip1 repression. Mol Cell Biol. 2004; 24:8813–8822. [PubMed: 15456857]

Olfert IM, Howlett RA, Tang K, Dalton ND, Gu Y, Peterson KL, Wagner PD, Breen EC. Muscle-specific VEGF deficiency greatly reduces exercise endurance in mice. J Physiol. 2009; 587:1755–1767. [PubMed: 19237429]

Oommen S, Gupta SK, Vlahakis NE. Vascular endothelial growth factor A (VEGF-A) induces endothelial and cancer cell migration through direct binding to integrin {alpha}9{beta}1: identification of a specific {alpha}9{beta}1 binding site. J Biol Chem. 2011; 286:1083–1092. [PubMed: 21071450]

Ota H, Akishita M, Eto M, Iijima K, Kaneki M, Ouchi Y. Sirt1 modulates premature senescence-like phenotype in human endothelial cells. J Mol Cell Cardiol. 2007; 43:571–579. [PubMed: 17916362]

Pearson KJ, Baur JA, Lewis KN, Peshkin L, Price NL, Labinskyy N, Swindell WR, Kamara D, Minor RK, Perez E, et al. Resveratrol delays age-related deterioration and mimics transcriptional aspects of dietary restriction without extending life span. Cell Metab. 2008; 8:157–168. [PubMed: 18599363]

Pette D, Staron RS. Myosin isoforms, muscle fiber types, and transitions. Microsc Res Tech. 2000; 50:500–509. [PubMed: 10998639]

Potente M, Ghaeni L, Baldessari D, Mostoslavsky R, Rossig L, Dequiedt F, Haendeler J, Mione M, Dejana E, Alt FW, et al. SIRT1 controls endothelial angiogenic functions during vascular growth. Genes Dev. 2007; 21:2644–2658. [PubMed: 17938244]

Price NL, Gomes AP, Ling AJ, Duarte FV, Martin-Montalvo A, North BJ, Agarwal B, Ye L, Ramadori G, Teodoro JS, et al. SIRT1 is required for AMPK activation and the beneficial effects of resveratrol on mitochondrial function. Cell Metab. 2012; 15:675–690. [PubMed: 22560220]

Prior SJ, Ryan AS, Blumenthal JB, Watson JM, Katzel LI, Goldberg AP. Sarcopenia Is Associated With Lower Skeletal Muscle Capillarization and Exercise Capacity in Older Adults. J Gerontol A Biol Sci Med Sci. 2016; 71:1096–1101. [PubMed: 26888434]

Ramsey KM, Mills KF, Satoh A, Imai S. Age-associated loss of Sirt1-mediated enhancement of glucose-stimulated insulin secretion in beta cell-specific Sirt1-overexpressing (BESTO) mice. Aging Cell. 2008; 7:78–88. [PubMed: 18005249]

Respress JL, Wehrens XH. Transthoracic echocardiography in mice. J Vis Exp. 2010

Rose P, Dymock BW, Moore PK. GYY4137, a novel water-soluble, H2S-releasing molecule. Methods Enzymol. 2015; 554:143–167. [PubMed: 25725521]

Ross JM. Visualization of mitochondrial respiratory function using cytochrome c oxidase/succinate dehydrogenase (COX/SDH) double-labeling histochemistry. J Vis Exp. 2011:e3266. [PubMed: 22143245]

Ryan NA, Zwetsloot KA, Westerkamp LM, Hickner RC, Pofahl WE, Gavin TP. Lower skeletal muscle capillarization and VEGF expression in aged vs. young men. J Appl Physiol (1985). 2006; 100:178–185. [PubMed: 16166239]

Salminen A, Kaarniranta K, Kauppinen A. Crosstalk between Oxidative Stress and SIRT1: Impact on the Aging Process. Int J Mol Sci. 2013; 14:3834–3859. [PubMed: 23434668]

Satoh A, Brace CS, Rensing N, Cliften P, Wozniak DF, Herzog ED, Yamada KA, Imai S. Sirt1 extends life span and delays aging in mice through the regulation of Nk2 homeobox 1 in the DMH and LH. Cell Metab. 2013; 18:416–430. [PubMed: 24011076]

Sinclair DA, Guarente L. Small-molecule allosteric activators of sirtuins. Annu Rev Pharmacol Toxicol. 2014; 54:363–380. [PubMed: 24160699]

Suo R, Zhao ZZ, Tang ZH, Ren Z, Liu X, Liu LS, Wang Z, Tang CK, Wei DH, Jiang ZS. Hydrogen sulfide prevents H(2)O(2)-induced senescence in human umbilical vein endothelial cells through SIRT1 activation. Mol Med Rep. 2013; 7:1865–1870. [PubMed: 23588928]

Turner N, Hariharan K, TidAng J, Frangioudakis G, Beale SM, Wright LE, Zeng XY, Leslie SJ, Li JY, Kraegen EW, et al. Enhancement of muscle mitochondrial oxidative capacity and alterations in insulin action are lipid species dependent: potent tissue-specific effects of medium-chain fatty acids. Diabetes. 2009; 58:2547–2554. [PubMed: 19720794]

Uddin GM, Youngson NA, Sinclair DA, Morris MJ. Head to Head Comparison of Short-Term Treatment with the NAD(+) Precursor Nicotinamide Mononucleotide (NMN) and 6 Weeks of Exercise in Obese Female Mice. Front Pharmacol. 2016; 7:258. [PubMed: 27594836]

Ungvari Z, Bagi Z, Feher A, Recchia FA, Sonntag WE, Pearson K, de Cabo R, Csiszar A. Resveratrol confers endothelial protection via activation of the antioxidant transcription factor Nrf2. Am J Physiol Heart Circ Physiol. 2010; 299:H18–24. [PubMed: 20418481]

van Beijnum JR, Rousch M, Castermans K, van der Linden E, Griffioen AW. Isolation of endothelial cells from fresh tissues. Nat Protoc. 2008; 3:1085–1091. [PubMed: 18546599]

Wang H, Listrat A, Meunier B, Gueugneau M, Coudy-Gandilhon C, Combaret L, Taillandier D, Polge C, Attaix D, Lethias C, et al. Apoptosis in capillary endothelial cells in ageing skeletal muscle. Aging Cell. 2014; 13:254–262. [PubMed: 24245531]

Wang X, Lockhart SM, Rathjen T, Albadawi H, Sorensen D, O'Neill BT, Dwivedi N, Preil SR, Beck HC, Dunwoodie SL, et al. Insulin Downregulates the Transcriptional Coregulator CITED2, an Inhibitor of Proangiogenic Function in Endothelial Cells. Diabetes. 2016

Wei T, Huang G, Gao J, Huang C, Sun M, Wu J, Bu J, Shen W. Sirtuin 3 Deficiency Accelerates Hypertensive Cardiac Remodeling by Impairing Angiogenesis. J Am Heart Assoc. 2017:6.

Wu D, Hu Q, Liu X, Pan L, Xiong Q, Zhu YZ. Hydrogen sulfide protects against apoptosis under oxidative stress through SIRT1 pathway in H9c2 cardiomyocytes. Nitric Oxide. 2015; 46:204–212. [PubMed: 25461268]

Yoshino J, Mills KF, Yoon MJ, Imai S. Nicotinamide mononucleotide, a key NAD(+) intermediate, treats the pathophysiology of diet- and age-induced diabetes in mice. Cell Metab. 2011; 14:528–536. [PubMed: 21982712]

Zhang H, Ryu D, Wu Y, Gariani K, Wang X, Luan P, D'Amico D, Ropelle ER, Lutolf MP, Aebersold R, et al. NAD(+) repletion improves mitochondrial and stem cell function and enhances life span in mice. Science. 2016; 352:1436–1443. [PubMed: 27127236]

Zhang Y, Jiang G, Sauler M, Lee PJ. Lung endothelial HO-1 targeting in vivo using lentiviral miRNA regulates apoptosis and autophagy during oxidant injury. FASEB J. 2013; 27:4041–4058. [PubMed: 23771928]

Zheng M, Qiao W, Cui J, Liu L, Liu H, Wang Z, Yan C. Hydrogen sulfide delays nicotinamide-induced premature senescence via upregulation of SIRT1 in human umbilical vein endothelial cells. Mol Cell Biochem. 2014; 393:59–67. [PubMed: 24729176]

Zu Y, Liu L, Lee MY, Xu C, Liang Y, Man RY, Vanhoutte PM, Wang Y. SIRT1 promotes proliferation and prevents senescence through targeting LKB1 in primary porcine aortic endothelial cells. Circ Res. 2010; 106:1384–1393. [PubMed: 20203304]

HIGHLIGHTS

- Reduced blood flow with age is due to loss of endothelial NAD^+-SIRT1 activity
- NAD^+ and H_2S control muscle angiogenesis and increase endurance in old mice
- The NAD precursor NMN mimics and augments exercise by inhibiting NICD-Notch
- Neovascularization is as important as mitochondria for rejuvenating muscle

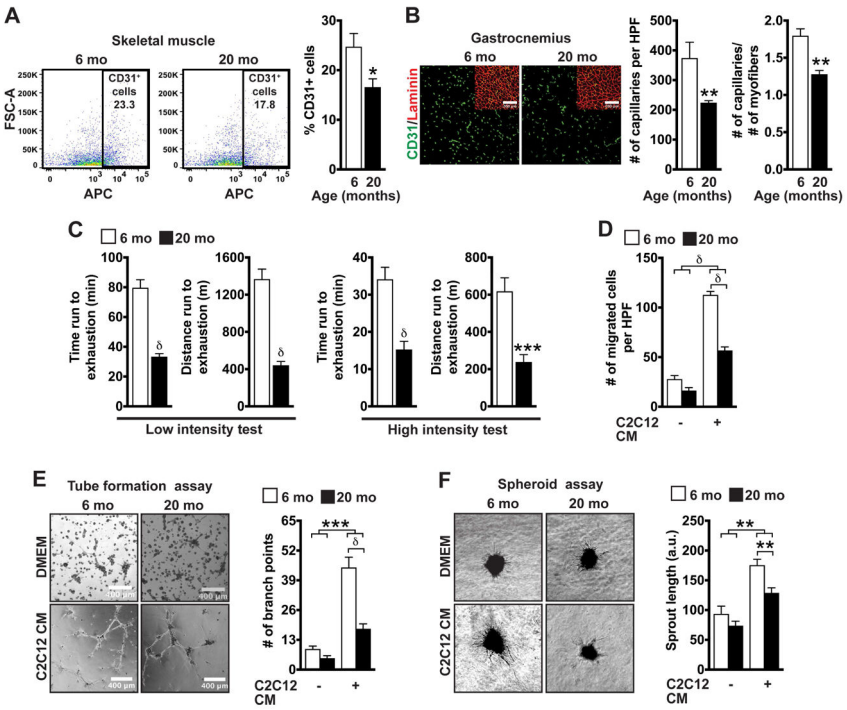

Figure 1. Aging is associated with decreased muscle angiogenesis and endurance

(A) Flow cytometry plots and percent $CD31^+$ ECs in skeletal muscle of young and old mice (n = 7).

(B) Gastrocnemius sections (@20X) showing CD31 and laminin staining. Number of capillaries and capillary/fiber ratio per high power field (HPF) (n = 7).

(C) Duration and distance run by mice until exhaustion (n = 11).

(D) Number of migrated MLECs in a transwell (n = 10).

(E) Images and number of branch points of tube networks formed by MLECs (n = 8).

(F) Images and sprout length of MLEC spheroids (n = 10).

Data expressed as mean ± SEM. *p < 0.05, **p < 0.005, ***p < 0.0005, $^{\delta}$p < 0.00005 by Student's t test (A–C) or two-way ANOVA with Bonferroni's correction (D–F). See also Figure S1

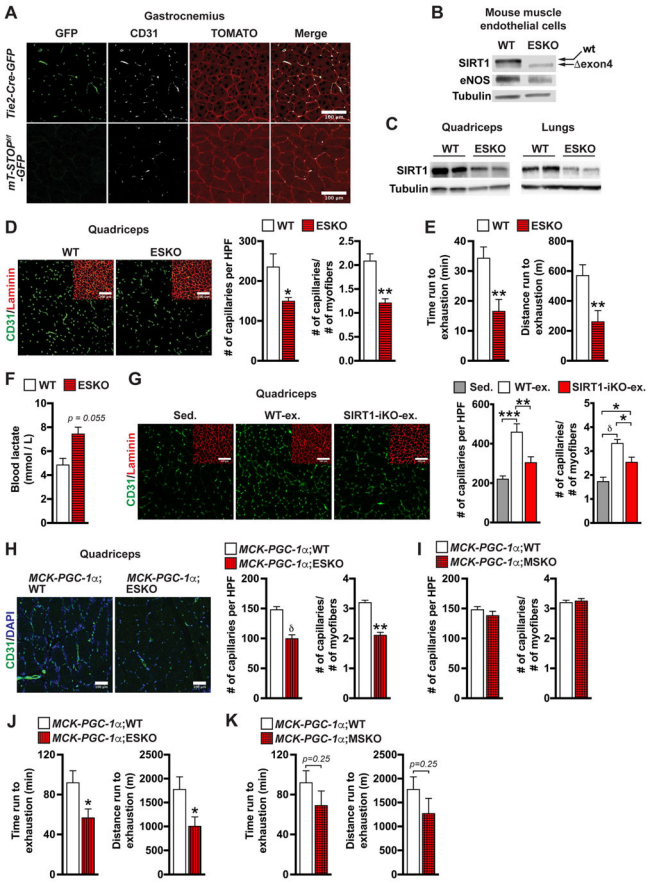

Figure 2. Endothelial SIRT1 deletion mimics the effect of aging on capillary density and endurance

(A) Gastrocnemius sections (@40X) showing GFP, CD31 and mTOMATO protein expression.

(B) SIRT1 and eNOS protein abundance in ECs isolated from skeletal muscle of WT and ESKO mice. SIRT1 exon 4 excision in ESKO results in SIRT1 band (Δ exon4) running slightly below the WT band. Tubulin serves as a loading control.

(C) SIRT1 protein in lung and quadriceps. Tubulin serves as a loading control.

(D) Quadriceps sections (@20X) showing CD31 and laminin staining. Number of capillaries and capillary/fiber ratio (6-month old, n = 8).

(E) Duration and distance run until exhaustion in a high intensity treadmill test (6-month old, n = 8).

(F) Post-exercise serum lactate levels (6-month old, n = 5).

(G) Quadriceps sections (@20X) from sedentary (SIRT1-iKO + WT) and exercised mice showing CD31 and laminin staining. Number of capillaries and capillary/fiber ratio (10-month old, n = 6).

(H) Quadriceps sections (@40X) showing DAPI and CD31 staining. Number of capillaries and capillary/fiber ratio (4-month old, n = 6).

(I) Number of capillaries and capillary/fiber ratio in the quadriceps (4-month old, n = 6).

(J) Duration and distance run until exhaustion in high intensity treadmill test (4-month old, n = 7).

(K) Duration and distance run until exhaustion in high intensity treadmill test (4-month old, n = 7).

Data expressed as mean ± SEM. *p < 0.05, **p < 0.005, ***p < 0.0005, $^{\delta}$p < 0.00005 by Student's t test (D–F and H, J, K) or one-way ANOVA with Bonferroni's corrections (G). See also Figure S2 and Movie 1

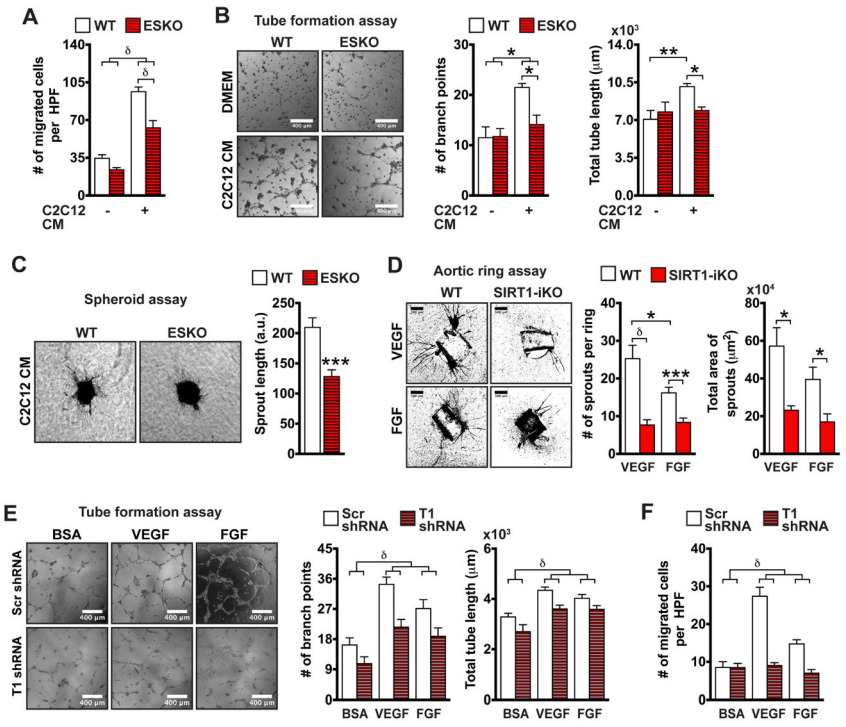

Figure 3. SIRT1 is required for angiogenesis *in vitro*

(A) Number of migrated MLECs (n = 12).

(B) Images, number of branch points and length of tube networks formed by MLECs (n = 5).

(C) Images and sprout length of MLEC spheroids (n = 8).

(D) Images, number and total area of microvessel sprouts in aortic rings (n = 8).

(E) Images, number of branch points and length of tube networks formed by HAECs infected with lentivirus expressing scrambled (Scr) or SIRT1 (T1) shRNA (n = 8).

(F) Number of migrated HAECs (n = 8).

Data are expressed as mean ± SEM. *p < 0.05, **p < 0.005, ***p < 0.0005, $^{\delta}$p < 0.00005 by Student's t test (C), one-way (D–F) or two-way (A–B) ANOVA with Bonferroni's corrections. See also Figure S3

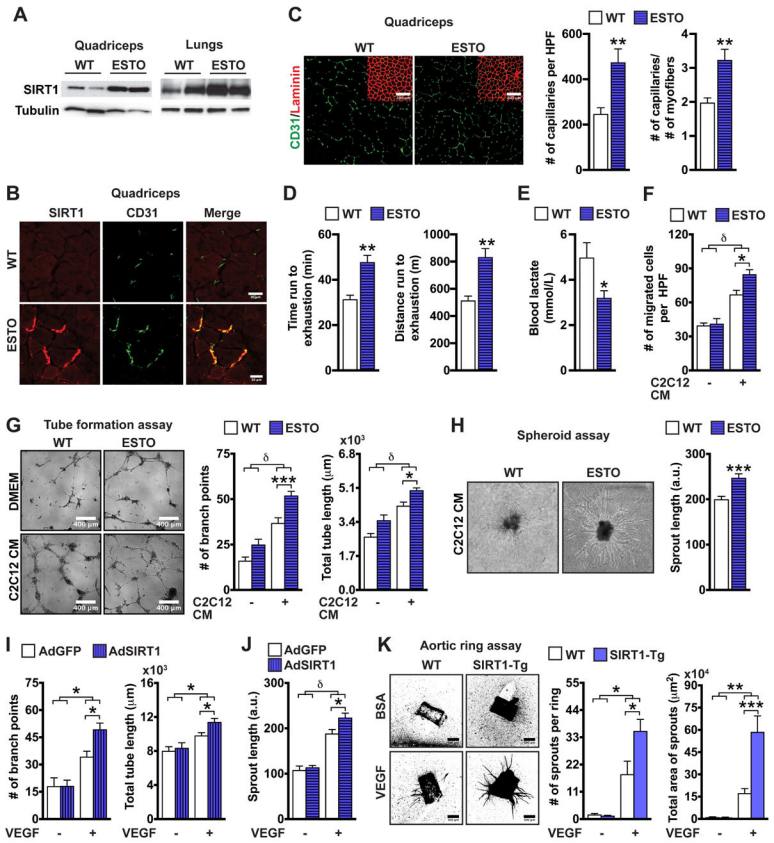

Figure 4. Endothelial SIRT1 increases capillary density and exercise capacity

(A) SIRT1 protein abundance in quadriceps and lungs. Tubulin serves as a loading control.

(B) Quadriceps sections (@60X) showing SIRT1 and CD31 expression.

(C) Quadriceps sections (@20X) showing CD31 and laminin staining. Number of capillaries and capillary/fiber ratio (6-month old, n = 8).

(D) Duration and distance run until exhaustion in a high intensity treadmill test (6-month old, n = 8).

(E) Post-exercise blood lactate levels (n = 5).

(F) Number of migrated MLECs (n = 10).

(G) Images, number of branch points and length of tube networks formed by MLECs (n = 8).

(H) Images and sprout length of MLEC spheroids (n = 8–9).

(I) Images, number of branch points and length of tube networks formed by HUVECs infected with adenovirus expressing GFP or SIRT1 (n = 8–9).

(J) Sprout length of HUVEC spheroids (n = 8).

(K) Images, number and total area of microvessel sprouts in aortic rings (n = 9).

Data expressed as mean ± SEM. *$p < 0.05$, **$p < 0.005$, ***$p < 0.0005$, $^{\delta}p < 0.00005$ by Student's t test (C–E and H) or two-way ANOVA with Bonferroni's corrections (F, G and I–K). See also Figure S4 and Movie 2

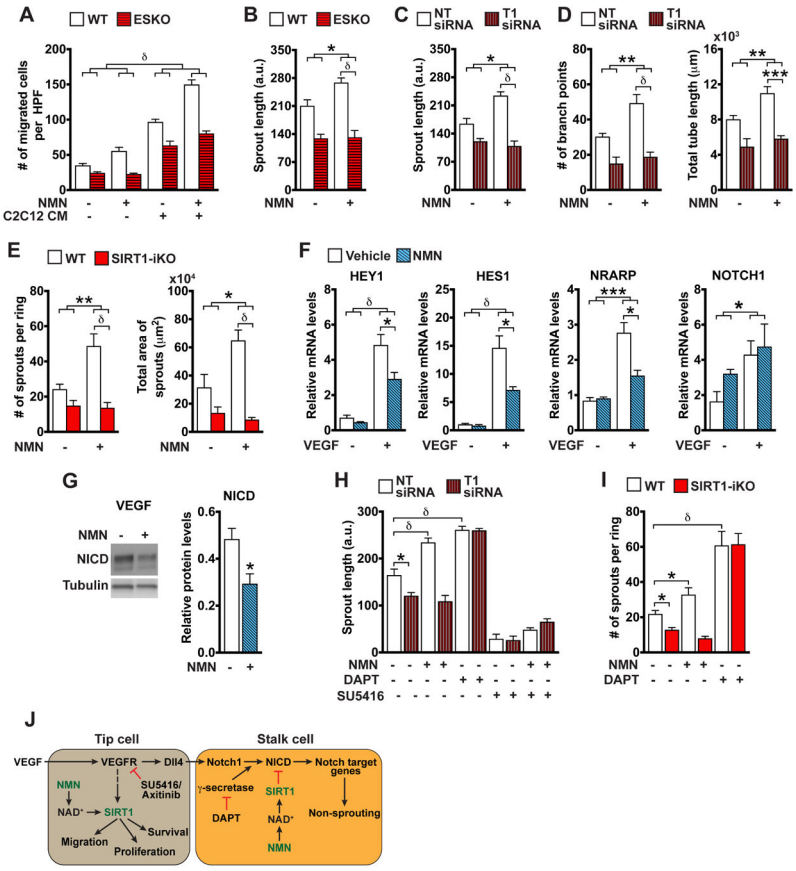

Figure 5. Endothelial NAD$^+$ sensitizes ECs to VEGF by suppressing Notch

(A) Number of migrated MLECs (n = 12).

(B) Sprout length of MLEC spheroids (n = 8).

(C) Sprout length of HAEC spheroids transfected with non-targeting (NT) or SIRT1 (T1) siRNAs (n = 8).

(D) Number of branch points and length of HAEC tube networks (n = 13).

(E) Number and total area of sprouts originating from aortic rings (18-month old, n = 8).

(F) Relative mRNA levels of Notch target genes (HEY1, HES1 and NRARP) and NOTCH1 in HAECs stimulated with VEGF for 1 hr (n = 4).

(G) Notch Intracellular Domain (NICD) protein and relative abundance in HAECs stimulated with VEGF for 5 hrs (n = 3).

(H) Sprout length of VEGF-stimulated HAEC spheroids transduced with NT or T1 siRNAs (n = 8).

(I) Number of sprouts in VEGF-stimulated aortic rings (18-month old, n = 8).

(J) VEGF stimulation during sprouting angiogenesis upregulates expression of Dll4 ligand in the tip cells, activating Notch in the stalk cells, which triggers proteolytic cleavage of Notch receptor by γ-secretase complex to release NICD from the cell membrane so it translocates to the nucleus and induces transcription of target genes. Activation of SIRT1 by the NAD booster NMN promotes migration, proliferation and survival in VEGF-stimulated ECs. In stalk cells, NMN suppresses NICD during VEGF/Dll4 stimulation and Notch target

gene activation, thereby promoting sprouting. VEGF receptor inhibitors SU5416 or axitinib block the effects of NMN on angiogenesis.

Data expressed as mean ± SEM. *$p < 0.05$, **$p < 0.005$, ***$p < 0.0005$, $^{\delta}p < 0.00005$ by Student's t test (G), one-way (H and I) or two-way (A–F) ANOVA with Bonferroni's corrections. See also Figure S5, Movie 3 and Movie 4

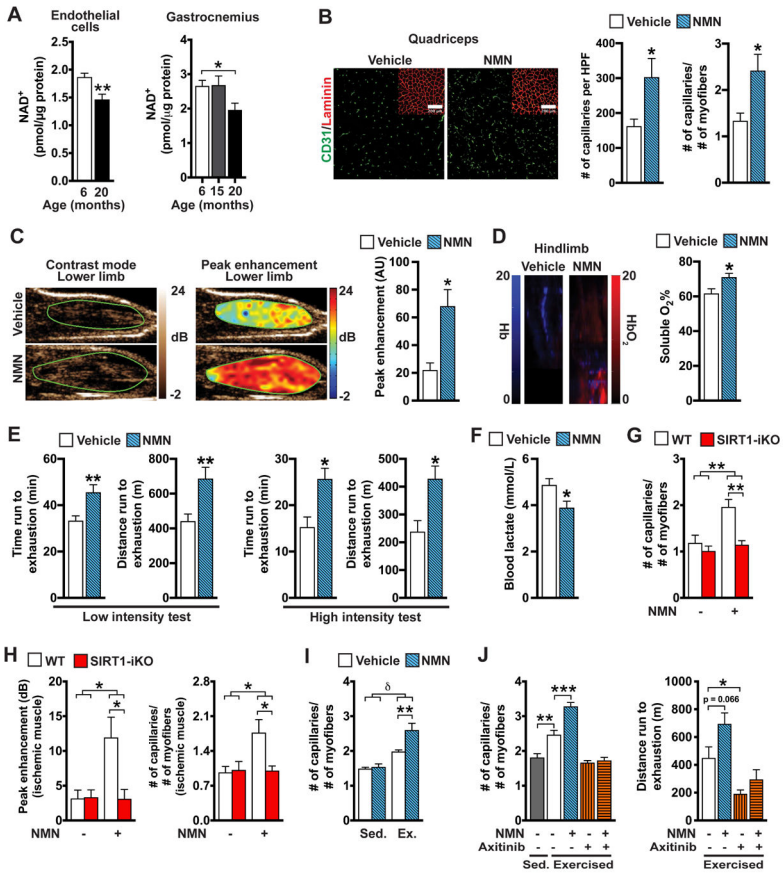

Figure 6. NAD repletion restores the microvasculature and exercise capacity of old mice

(A) NAD^+ levels in MLECs (n = 6) and gastrocnemius muscles (n = 10) isolated from 6 and 20-month old mice.

(B) Quadriceps sections (@20X) from 20-month old vehicle or NMN-treated mice showing CD31 and laminin staining. Number of capillaries and capillary/myofiber ratio (n = 8).

(C) Contrast-mode and peak enhancement-mode contrast-enhanced ultrasound images of mouse hindlimb. Quantification of peak enhancement (20-month old, n = 5).

(D) Total hemoglobin (Hb) and oxygenated Hb (HbO_2) mean intensity in the hindlimbs of mice measured using photoacoustics tomography. Percent soluble O_2 levels (n = 13).

(E) Duration and distance run until exhaustion (20-month old, n = 13).

(F) Post-exercise blood lactate levels (20-month old, n = 13). (G) Capillary/myofiber ratio in gastrocnemius sections (20-month old, n = 5).

(H) Peak enhancement and capillary/myofiber ratio for ischemic hindlimbs (8-month old, n = 5).

(I) Capillary/myofiber ratio in quadriceps of sedentary or exercised mice (10-month old, n = 5).

(J) Capillary/myofiber ratio in quadriceps (5-month old, n = 5). Distance run until exhaustion at the end of the exercise paradigm (n = 5).

Data are expressed as mean ± SEM. *$p < 0.05$, **$p < 0.005$, ***$p < 0.0005$, $^{\delta}p < 0.00005$ by Student's t test (A–F), one-way (J) or two-way (G–I) ANOVA with Bonferroni's corrections. See also Figure S6 and Movie 5

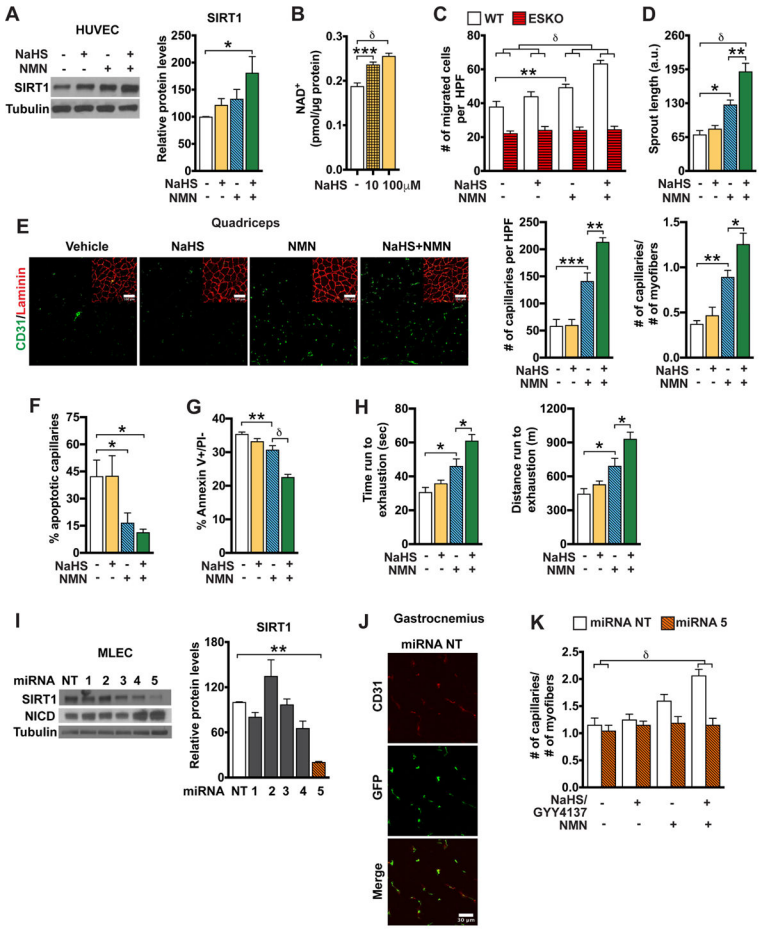

Figure 7. Exogenous hydrogen sulfide activates SIRT1 and augments the effects of NMN

(A) SIRT1 protein and relative abundance in HUVECs treated for 24 hrs (n = 4).

(B) NAD^+ levels in HUVECs treated for 24 hrs (n = 6).

(C) Number of migrated MLECs stimulated with C2C12 CM for 12 hrs (n=15).

(D) Sprout length of VEGF-stimulated HUVEC spheroids (n = 7).

(E) Quadriceps sections (@20X) showing CD31 and laminin staining. Capillary number and capillary/myofiber ratio (32-month old, n = 7).

(F) Percent TUNEL+ capillaries in quadriceps sections (32-month old, n = 5).

(G) Number of apoptotic HUVECs (Annexin V+/PI−) following exposure to H_2O_2 (n = 12).

(H) Duration and distance run until exhaustion in a low intensity treadmill test (32-month old, n = 7).

(I) SIRT1 and NICD proteins in MLECs transduced with lentiviruses expressing NT or SIRT1 miRNAs (miRNA # 1–5). Relative SIRT1 protein abundance (n = 3).

(J) Images of gastrocnemius sections (@40X) immunostained with EGFP and CD31 from WT mice injected with lentiviral particles that transduced EGFP and NT miRNA.

(K) Capillary/myofiber ratio in the gastrocnemii of mice infected with lentiviral particles transducing NT or SIRT1 # 5 miRNA (n = 6).

Data are expressed as mean ± SEM. *p < 0.05, **p < 0.005, ***p < 0.0005, $^{\delta}$p < 0.00005 by Student's t test (I), one-way (A–B and D–H) or two-way (C and K) ANOVA with Bonferroni's corrections. See also Figure S7 and Table S1